Green tea polyphenol-reduced graphene oxide: Derivatisation, reduction efficiency, reduction mechanism and cytotoxicity

M. F. Abdullah[a, b], R. Zakaria[a], S. H. S. Zein[a, c,*]

[a]*School of Chemical Engineering, Engineering Campus, UniversitiSains Malaysia, 14300, Seri Ampangan, NibongTebal, SeberangPerai Selatan, Pulau Pinang, Malaysia*
[b]*School of Bioprocess Engineering, Universiti Malaysia Perlis, Kompleks Pusat Pengajian Jejawi 3, 02600, Arau, Perlis, Malaysia*
[c]*Department of Engineering, University of Hull, HU6 7RX, Hull, United Kingdom*

* Corresponding author. Tel.: +44 (0) 1482 466753.
E-mail address: S.H.Zein@hull.ac.uk (S.H.S Zein).

This paper reports on the derivatisation, reduction efficiency, reduction mechanism and cytotoxicity of green tea polyphenol-reduced graphene oxide (GTP-RGO). The reduction of graphene oxide (GO) at 90°C using a weight ratio (WR) of GTP/GO=1 resulted in the production of a stable GTP-RGO dispersion in aqueous media, as indicated by the results of ultraviolet-visible (UV-Vis) spectroscopy, Fourier transform infrared (FTIR) spectroscopy, thermogravimetric analysis (TGA) and the measurement of zeta potential and electrophoretic mobility. In addition, the results from UV-Vis spectroscopy and X-ray photoelectron spectroscopy (XPS) analysis indicated the comparable reduction ability of GTP relative to the standard reducing agent, hydrazine (N_2H_4). The removal mechanism of epoxy group from GO via reduction reaction with GTP was investigated by implementing hybrid functional method of Becke-3-parameters-Lee-Yang-Parr (B3LYP)using Gaussian 09 software. The energy and frequency calculations showed that the GO reduction using GTP was more spontaneous and relatively took place faster than the reduction using N_2H_4, as evidenced by higher entropy change (ΔS) (0.039 kcal/mol·K) and lower Gibbs free energy (ΔG) barrier (58.880 kcal/mol).The cytotoxicities of GO and GTP-RGO samples were evaluated against human colonic fibroblasts cells (CCD-18Co). The GO sample was determined to be toxic even at low concentration (6.25 µg/mL), while the GTP-RGO sample possesses notably low toxicity at the same concentration. The cell culture experiments revealed that the incorporation of GTP led to a decrease in the toxicity of GTP-RGO samples.

Keywords: graphene oxide, reduced graphene oxide, green tea polyphenol, reduction mechanism, cytotoxicity

1. Introduction

Graphene, a unique two-dimensional (2D) nanostructure, has garneredsubstantial attention from researchers in a variety of applications including nanoelectronics[1], sensors[2],

energy storage [3] and biomedical applications[4] due to its intriguing and exceptional physicochemical properties[5-7].Graphene and its derivatives have been widely reported to be produced via a number of versatile techniques, including the micromechanical cleavage of highly oriented pyrolytic graphite (HOPG) using adhesive tape[8], the decomposition of hydrocarbon on transition metal surfaces using chemical vapour deposition (CVD) technique [9], the thermal decomposition of silicon carbide (SiC) through high-temperature annealing [10] and the reduction of graphene oxide (GO). Among these methods, the reduction of GO is the most promising and efficient route for graphene production owing to its cost-effectiveness, scalability for mass production, versatility for chemical functionalisation, and simplicity of equipment setup and reaction procedures[11, 12].

The chemical reduction of GO with various chemical-based reducing agents, such as hydrazine (N_2H_4)[13, 14], hydroquinone ($C_6H_4(OH)_2$)[15] and sodium borohydride ($NaBH_4$)[16]to remove oxygen functional groups (i.e., epoxide (–O–), hydroxyl (–OH), carbonyl (–C═O) and carboxyl (–COOH)) in GO has attracted considerable attention. Although N_2H_4 is known to be the most widely used and effective reducing agent for the chemical reduction of GO, it is highly corrosive and toxic[17, 18]. Hence, an environmentally friendly and effective agent for the reduction of GO is desirable.

For many years, green tea has been utilised as a common beverage offering enormous health benefits including the prevention of cancer and heart disease, the lowering of high blood pressure, and reduction of high blood cholesterol concentrations [19, 20]. However, only recently has green tea attracted significant interest for its application in production of nanomaterials and nanocomposites. Green tea possesses the highest composition of a polyphenolic compound, which was regarded as an effective reducing agent due to its ability to donate an electron or hydrogen atom easily [21]. It has been reported that the reductive property of green tea polyphenol (GTP) has enabled its use in the synthesis of metal nanoparticles, such as palladium (Pd), gold (Au), and silver (Ag) [22-24], and the production of well-dispersed single-wall carbon nanotubes (SWCNTs) in water [25].

In this regard, it is highly probable that the reduction of GO and the preparation of a stable dispersion of reduced GO (RGO) could be achieved using GTP. However, despite its importance, the reduction mechanism of GO using GTP remains unclear mainly due to complex structures of GTP. We aimed to investigate the possible removal mechanism of epoxy groups from GO via reduction reaction with GTP through density functional theory (DFT) calculations. The employment of GTP for the reduction of GO may also open possibilities for the preparation of non-toxic RGO, allowing potential applications in the biomedical field. To achieve the exciting potential of RGO in biomedical applications, we sought to investigate its potential toxicity in detail [7, 26].

In this study, we utilised GTP as a safer and environmentally friendly reducing agent for the reduction of GO. The GO and GTP-RGO samples were analysed using ultraviolet-visible (UV-Vis) spectroscopy, Fourier transform infrared (FTIR)spectroscopy, thermogravimetric analysis (TGA), X-ray photoelectron spectroscopy (XPS) and zeta potential, as well as electrophoretic mobility measurements. Accordingly, the removal mechanism of epoxy from GO by epigallocatechin gallate (EGCG), the most potent catechin in GTP was investigated by implementing hybrid functional theory of Becke-3-parameters-Lee-Yang-Parr (B3LYP) using Gaussian 09 software. To the best of our knowledge, the reduction mechanism of GO by GTP through computational study has yet been investigated. In addition, the cytotoxicities of GO and

GTP-RGO samples were evaluated against human fibroblast cells (CCD-18Co) to understand the potential toxicity and biocompatibility of these samples further.

2. Experimental

2.1. Materials

Graphite oxide powder (purity >99 wt%) was purchased from the Chinese Academy of Sciences, China. Green tea leaves extract powder (total polyphenol of 99.5%) was obtained from Guangzhou New Sino Biotech, China, while N_2H_4 solution (35 wt% in water) was purchased from Sigma Aldrich, Malaysia. Deionised (DI) water was used as dispersion medium. Nylon membrane (0.22 μm) was purchased from GE Healthcare Life Sciences, USA. CCD-18Co cells lines were obtained from American Type Culture Collection (ATCC), USA. Both Dulbecco's Modified Eagle's Medium (DMEM) and MTT salt solution were purchased from Invitrogen Life Technologies, Germany.

2.2. Preparation of RGO suspension

The aqueous suspension of GO consisted of 0.3 mg/mL commercially available graphite oxide powder in DI water. The graphite oxide sheets were dispersed ultrasonically in DI water for 200 seconds to exfoliate them into GO. Then, the GO suspension was centrifuged at 4000 rpm for 30 minutes to remove the unexfoliated graphite oxide sheets. The reduction reaction of GO with GTP was carried out in a 50 mL batch reactor-closed system. Typically, GTP with a weight ratio (WR) of GTP/GO=1was added to 30 mL of GO suspension. Subsequently, the reduction of GO was performed in the reactor for 8 hours at 90°C while the GO-GTP mixture was stirred continuously at 200 rpm during the reduction reaction. The suspension of the final products was filtered through a nylon membrane (0.22 μm) and washed 3-5 times with DI water to collect the resultant GTP-RGO sheets. A stable suspension of GTP-RGO (GTP-RGO-WR1) was prepared by dispersing the resultant GTP-RGO sheets in DI water through sonication while maintaining the concentration at 0.3 mg/mL. Meanwhile, the GO suspension was also reduced using N_2H_4 solution for 8 hours under similar reduction conditions (WR of N_2H_4/GO=1, 90°C)to compare the reduction efficiency of GTP with the efficiency of N_2H_4 as a standard reducing agent. Thus, the produced RGO using N_2H_4 solution was referred as N_2H_4-RGO-WR1.

2.3. Sample characterisation

The UV-Vis absorption spectra of GO and RGO samples were recorded over a wavelength range of 200-700 nm using Agilent Technologies Cary-60 UV-Vis spectrophotometer to monitor the reduction reaction of GO. The FTIR analysis was conducted to determine the presence of specific oxygen functional groups in GO and RGO samples. The FTIR spectra were recorded over a frequency range of 600 to 4000 cm^{-1}using a Shimadzu IR Prestige -21 FTIR spectrophotometer. TGA was performed to evaluate the thermal stability of GO and RGO samples. TGA was carried out under an air atmosphere with a heating rate of 10°C/minute using a TGA7 Perkin Elmer Pyris instrument. The variation of chemical states of GO and RGO samples were examined by XPS analysis. The XPS spectra were recorded using a high resolution, multi techniques X-ray spectrometer (Axis Ultra DLD XPS Model Kratos). The

stability of GO and RGO suspensions were examined by measuring the zeta potential and electrophoretic mobility using Malvern Instruments Nano Series Zetasizer (ZEN 3600).

2.4 Reduction mechanism of GO

All calculations involving the structures and energies were computed using Gaussian 09 software [27]. Numerous theoretical studies have shown that most of the oxygen atoms were adsorbed above the C-C bond across the basal plane of graphite to form epoxy groups during the oxidation of graphite[28, 29]. Hence, the GO was modelled as a fragment of graphene sheet decorated with epoxy groups while the structure of EGCG was used to represent GTP in this computational study. The structures of all the reactants (i.e., GO with epoxide group and GTP (EGCG)) and the predicted products (i.e., GTP-RGO-WR1, galloyl-derived orthoquinone and water) that involved in the GO reduction were illustrated schematically in Fig. 1. In this computational study, the GO reduction process was represented by the removal of epoxy groups from GO structure through the transfer of hydrogen atoms from the gallic acid unit (ring D) in EGCG. The other structures in EGCG (i.e., ring A, ring B and ring C) were denoted as R for simplification in illustration purpose. Initially, all of the geometrical structures were modelled using GaussView 5 software prior structural optimization using hybrid functional theory of B3LYP combined with the 3-21G basis set. Subsequently, the thermodynamic quantities including the enthalpy change (ΔH), entropy change (ΔS) and the Gibbs free energy change (ΔG) were calculated by performing frequency analysis at the same level of functional theory (B3LYP/3-21G) using Gaussian 09 software. Similar optimization and frequency calculations were computed for GO reduction using N_2H_4 to compare the reduction efficiency between the two reagents. A singlet spin-restricted B3LYP method was applied in all of the optimization and frequency calculations.

2.5. Cytotoxicity testing

The cytotoxicity of GO and GTP-RGO-WR1 samples were examined against CCD-18Co cells by inoculating and exposing the cells to concentrations of GO and GTP-RGO-WR1 samples ranging from 6.25-200 μg/mL. Meanwhile, another GTP-RGO suspension was produced by using WR of GTP/GO=5 (GTP-RGO-WR5); this GTP-RGO suspension was also subjected to cytotoxicity testing to investigate the effect of the incorporation of a higher amount of GTP on the toxicological behaviour of the GTP-RGO suspension.

2.5.1. Cells culture

The CCD-18Co cells were cultured in DMEM supplemented with 10% fetal bovine serum (FBS). The cells were incubated in a humidified incubator (5% CO_2, 37°C) until the cells reached 70% confluency in the flask.

2.5.2. Cells seeding

The cultured cells were seeded in 96-well plates (1.5×10^5 cells per well) and allowed to attach for 24 hours before further treatment was made. The GO and GTP-RGO suspensions (GTP-RGO-WR1 and GTP-RGO-WR5) were diluted using cell culture medium to achieve the

desired concentrations of 6.25, 12.5, 25, 50, 100 and 200 μg/mL.100 μL of the medium containing GO and GTP-RGO particles with different concentrations were added into each well of the 96-well plates. For comparison, 100 μL of cell culture medium with no particles was added to the control well (untreated cells).

2.5.3. MTT viability assay

The viability of the CCD-18Co cells treated with different concentrations of GO and GTP-RGO suspensions was evaluated colourimetrically using an MTT assay. MTT salt solution was added 4 hours before the end of the 72-hour sample incubation. The cell culture medium and the MTT solution were aspirated while the formazan solubilisation buffer was added to the wells. The plate was incubated for another 5 minutes (37°C) before the absorbance was measured at 570 nm using an Ascent Multiskan ELISA microplate reader. All samples were examined in triplicate (n = 3). The percentage of cell inhibition was determined using the optical density (O.D.) values by employing Eq. (1)[30, 31]:

$$\% \text{ Cell inhibition} = \frac{\text{O.D. value (control cell)} - \text{O.D. value (treated cell)}}{\text{O.D. value (control cell)}} \times 100 \quad (1)$$

3. Results and Discussion

3.1. Monitoring the reduction reaction of GO with GTP

Physical observation is the first indication and the most direct way to determine the successful reduction of GO. Post reduction reaction with GTP (WR of GTP/GO=1, 90°C), the colour of GO suspension was observed to change from yellow-brownish to black colour as shown in Fig. 2(a). This observation was presumably due to the partial re-graphitisation of GO and the increased concentration of the GTP-RGO-WR1 suspension as a result of the eradication of oxygen functionalities [32, 33]. To monitor the reduction reaction of GO with GTP, the UV-Vis absorption spectra of GTP-RGO-WR1 were recorded as a function of reaction time (Fig. 2(b)). As depicted in Fig. 2(b), a maximum peak at 228 nm was observed from the absorption spectrum of GO. The absorption peak at 228 nm could be assigned to the π-π transitions of aromatic C=C bonds and C=O bonds [34]. As the reaction progressed, the absorption peak of GO was shifted towards higher wavelengths (271 nm) indicates that the GO has been reduced and the sp^2 bonding network of GO has been re-established. Apart from the absorption peaks at 271 nm, the GTP-RGO-WR1 samples also exhibit strong absorption peaks at 206 nm. These peaks correspond to the structure of the benzene ring in EGCG, which is the most potent catechin in GTP [35]. The absorption peaks at 206 nm were observed in all of the UV-Vis spectra of GTP-RGO-WR1 samples even after those samples went through 3-5 washes signifying the strong adsorption between GTP and GTP-RGO-WR1. This strong interaction may be the key factor that influences the stability of GTP-RGO-WR1 suspension.

In addition, the UV-Vis absorption intensity of the resulting GTP-RGO-WR1 suspension was observed to increase with increasing reaction time. According to Beer's law, there is a linear correlation between the absorption intensity and the concentration of an absorbing species[36]. When the reaction time increases, the number of oxygen functionalities eliminated from GO multiplies. This led to an increase in the concentration of the resulting GTP-RGO-WR1

suspension, which may explain the increase of the absorption intensity of GTP-RGO-WR1 suspension with increasing reaction times. However, a nearly constant absorption intensity of GTP-RGO-WR1 suspension was observed at a reaction time of 6 to 8 hours. At a longer reaction time (>6 hours), most of the oxygen functionalities of GO may already have been removed. Thus, there is little or no further increase in the concentration of GTP-RGO-WR1, resulting in an similar absorption intensities of GTP-RGO-WR1 samples produced at 6 to 8 hours.

The effective removal of oxygen functionalities from GO via reduction reaction with GTP was reflected by the FTIR and TGA spectra. The FTIR spectra of GO and GTP-RGO-WR1 are presented in Fig. 3. The GO sample possesses multiple peaks between 1000 cm^{-1} to 1800 cm^{-1}; these peaks can be attributed to a variety of functional groups including hydroxyl (1061 cm^{-1}), epoxy (1233 cm^{-1}) and carboxyl groups (1727 cm^{-1}) [18, 37]. In addition, another peak was also observed at 1620 cm^{-1}whichcan be assigned to the skeletal vibration of unoxidised graphitic domains [37, 38]. Post reduction with GTP, the peaks belonging to hydroxyl, epoxy and carboxyl groups as well as the peak of the vibration of unoxidised graphitic domains disappeared, as shown in the FTIR spectrum of GTP-RGO-WR1. Additionally, new peaks emerged at 1597 cm^{-1} and 2104 cm^{-1}which were assigned to the cumulative double bond of the oxidised GTP [34]. This observation indicates successful reduction of GO by GTP.

Meanwhile, the thermal stability of GO and GTP-RGO-WR1 samples were evaluated by TGA in air atmosphere. Fig. 4shows the TGA curves of GO and GTP-RGO-WR1. A three-stage weight loss was observed from the TGA curve of GO. The first weight loss occurred below 100°C due to the vaporisation of moisture from the GO sample. The second weight loss of almost 22 wt% was observed to occur in the temperature range between 150-230°C. The significant weight loss in this temperature range was associated with decomposition of the oxygen functional group in GO [18, 37]. GO also underwent further weight loss in the between 450-565°C, primarily due to the burning of the graphitic regions [39, 40].The GTP-RGO-WR1sample, however, exhibits only a minor weight loss of 2.35 wt% from 150-230°C. This observation might indicate that most of the oxygen functionalities were successfully removed during the reduction reaction with GTP.

3.2. Reduction efficiency of GTP

Herein, we intend to compare the reduction efficiency of GTP with the efficiency of the standard reducer, N_2H_4which is known to be the most widely used and effective reducing agent for the chemical reduction of GO [14, 21]. However, the utilisation of N_2H_4 in GO reduction has been deterred due to its corrosive and toxic nature [17, 18]. Fernandez-Merino et al. [41] have suggested that the final position of the UV-Vis absorption peak can be used as an indicator to estimate reducing agent efficiency. Fig. 5 illustrates the UV-Vis absorption spectra of GTP-RGO-WR1 and N_2H_4-RGO-WR1. After an 8-hour reduction period, the final position of the absorption peaks of GTP-RGO-WR1 and N_2H_4-RGO-WR1 were observed at 271 nm and 267 nm, respectively. GTP-RGO-WR1 exhibits a nearly identical final absorption peak to N_2H_4-RGO-WR1 suggesting comparable reduction efficiency of GTP relative to N_2H_4.

Meanwhile, chemical state variations between GO, GTP-RGO-WR1 and N_2H_4-RGO-WR1 were evaluated using XPS analysis. The XPS spectra in the C1s region of GO, GTP-RGO-WR1 and N_2H_4-RGO-WR1 are depicted in Fig. 6. The C1s XPS spectrum of GO shows four different types of carbon components, namely, the sp^2 carbon (C-C, 284.8 eV), the carbon of the C-O bond (287.0 eV), the carbon of the carbonyl (C=O, 289.3 eV) and the carboxylate carbon

(O-C=O, 291.6 eV) [14, 18]. Although the C1s XPS spectrum of GTP-RGO-WR1 also exhibits the same oxygen functionalities (C-O, C=O and O-C=O), their intensities are much smaller than those ofGO. In addition, the intensity of the sp^2 carbon in GTP-RGO-WR1 was increased significantly compared with GO indicating the establishment of an sp^2 bonding network and the successful reduction of GO [14, 37]. Similarly, the intensities of oxygen functionalities in N_2H_4-RGO-WR1 were also reduced significantly compared to those of GO suggesting the successful removal of oxygen functionalities from GO byN_2H_4. The similar sp^2 intensities of N_2H_4-RGO-WR1 and GTP-RGO-WR1 indicate the comparable reduction property of GTP relative to the standard reducing agent, N_2H_4 [14, 18, 21].

A stable RGO suspension would facilitate further processing and expand the range of possible applications[11, 42]. Thus, the stability of the GO and RGO suspensions were examined by employing zeta potential and electrophoretic mobility measurements. Zeta potential provides imperative information regarding particle aggregation and the kinetic stability of the suspensions. Electrophoretic mobility is the velocity of a particle that moves under the influence of an electric field and it is associated with the zeta potential value. High absolute zeta potential and electrophoretic mobility values are desirable as they demonstrate production of a well-dispersed and stable suspension [43, 44]. Table 1 shows the zeta potential and electrophoretic mobility values of GO, GTP-RGO-WR1 and N_2H_4-RGO-WR1 suspensions. All measurements were carried out at pH=7. The high absolute zeta potential (-57.43 mV) and electrophoretic mobility values (-4.50 μmcm/Vs) listed in Table 1, support the conclusion that a well-dispersed and stable aqueous suspension of GO has been prepared. The high stability of the GO suspension was attributed to the electrostatic stabilisation [42], and the hydrophilic nature of GO [33].

The zeta potential and electrophoretic mobility values of the as-produced GTP-RGO-WR1 suspension were -39.43 mV and -3.09 μmcm/Vs, respectively. Everett [45] has suggested that absolute zeta potential values greater than 30 mV represent an adequate mutual repulsion which ensures the stability of a suspension. This result shows that GTP possesses the capability to reduce GO and to stabilise the as-produced RGO sheets. The increased stability of the GTP-RGO-WR1 suspension is most likely due primarily to the π-π interactions between the GTP and RGO layers [18, 34], in addition to the steric effect caused by the incorporation of GTP [46]. On the contrary, high agglomeration of N_2H_4-RGO-WR1 sheets was observed as the instability of RGO produced was clearly shown by low absolute zeta potential (-15.50 mV) and electrophoretic mobility values (-1.21 μmcm/Vs). This high agglomeration was reported to be due to an increase in the interlayer van der Waals interactions [14].

3.3 Reduction mechanism of GO by GTP

In this study, the possible reduction mechanism of GO by GTP was investigated using Gaussian 09 and GaussView 5 software. All of the input and output structures were modelled using GaussView 5 software while the subsequent calculations involving the structures and energies were computed using Gaussian 09 software. We found that the epoxide removal from GO was initiated by the ring opening of epoxy groups due to the transfer of hydrogen atom from EGCG in GTP. This mechanism was shown in Fig. 7. In the first step of this mechanism, the EGCG (ring D) attacks the sp^2 carbon located at the meta position of epoxide in GO (ring E) as portrayed in Fig. 7(a). One hydrogen atom was transferred from ring D to the oxygen atom of the epoxide group. In the meantime, GO rotates in a rotatory mode causing the epoxide group to revolve from the upper side to the lower side. The transfer of the hydrogen atom initiates the ring

opening of epoxide group and led to the formation of hydroxyl group as shown in Fig. 7(b). The C-O-C bond between ring D and ring E was formed, yielding intermediate structure as illustrated in Fig. 7(c). In the next step of this mechanism, another hydrogen atom was transferred from ring D to the hydroxyl group while the C-O-C bond between ring D and ring E was broken as shown in Fig. 7(d). This led to the formation of the products namely GTP-RGO-WR1, galloyl-derived orthoquinone and a water molecule (Fig. 7(e)).

We also investigating the reduction mechanism of GO by N_2H_4 using the same level of functional theory (B3LYP/3-21G) as we intend to compare the reduction efficiency of GTP to the standard reducing agent, N_2H_4. The mechanism of the epoxide removal using N_2H_4 was found to be similar to the mechanism using GTP. The equilibrium structures of GO with epoxide group and N_2H_4 were shown in Fig. 8(a). N_2H_4 attacks the sp^2 carbon nearest to the epoxide group from backside and transfers one hydrogen atom to the epoxide group, resulted in the initiation of ring opening of epoxide group and the formation of hydroxyl group as illustrated in Fig. 8(b). The hydrazino group ($-HNNH_2$) was attached to the ring E and formed intermediate structure (Fig. 8(c)). Another hydrogen atom was transferred from the hydrazino group to the hydroxyl group as shown in Fig. 8(d). This yields N_2H_4-RGO-WR1, cis-diazene (N_2H_2) and a water molecule as portrayed in Fig. 8(e).

Subsequently, the thermodynamic quantities (i.e., ΔS and ΔG) of the stationary points were calculated using frequency analysis tool which was incorporated within Gaussian 09 software. Table 2 shows the ΔH, ΔS and ΔG for all the stationary points involved in the GO reduction using GTP and N_2H_4 at 90°C. All the values of thermodynamic quantities for reactant were zero since all the values of thermodynamic quantities for other stationary points were defined based on the values of the reactant. Table 2 shows that the ΔH for GO reduction using GTP and N_2H_4 are -14.053 kcal/mol and -16.021 kcal/mol, respectively indicating that both of these reactions are exothermic. In the meantime, the frequency calculations reveal that the ΔS for the GO reduction using GTP and N_2H_4 are 0.039 kcal/mol·K and 0.035 kcal/mol·K, respectively. S is a state function in which it depends only on the initial and final state of the system, regardless of the path by which the changes take place [47]. A spontaneous process has a tendency for S to increase. From the result of the frequency calculations, the GO reduction using GTP was demonstrated to possess higher ΔS than the reduction using N_2H_4 indicating more spontaneous and more favourable reaction that likely to occur. Meanwhile, the step change from intermediate to transition state structure, ts2 was determined to be the rate-determining step for both the GO reduction using GTP and N_2H_4[48]. This step has G barrier of 52.880 kcal/mol and 99.692 kcal/mol for reduction using GTP and N_2H_4, respectively. The rate-determining step is the mechanism step with the greater energy barrier (i.e., the slowest step), thus this step has the greatest influence on the reaction rate[48]. The GO reduction using GTP was found to be more efficient and relatively took place faster than the reduction using N_2H_4 since the G barrier for GO reduction using GTP was lower than that of N_2H_4.

3.4. Cytotoxicity evaluation

The cytotoxicity of GO and GTP-RGO samples was investigated in terms of mitochondrial respiratory activity of CCD-18Co cells. We sought to evaluate the effect of concentration on the toxicological behaviour of GO and GTP-RGO samples. For this cytotoxicity evaluation, two GTP-RGO suspensions were prepared using WR of GTP/GO =1 (GTP-RGO-WR1) and WR of GTP/GO=5 (GTP-RGO-WR5) were subjected to cytotoxicity

testing. Both of these GTP-RGO suspensions were selected for this testing to examine the effect of higher GTP incorporation on the cytotoxicity of GTP-RGO suspension. The effect of different concentrations of GO, GTP-RGO-WR1, GTP-RGO-WR5 and GTP on the metabolic activity of CCD-18Co cells was shown in Fig. 9.

For GO, GTP-RGO-WR1 and GTP-RGO-WR5 samples, the MTT assays reveal that the percentage inhibition of cell proliferation was increased with increasing concentration of the test samples. GO sample inhibits almost 50% of CCD-18Co cell proliferation even at the lowest concentration (6.25 µg/mL). This indicates that the GO is toxic towards CCD-18Co cells. However, at a similar concentration (6.25 µg/mL), the percent inhibition of cell proliferation by GTP-RGO-WR1 was reduced significantly compared to GO. The decrease of the toxicological effect of GTP-RGO-WR1 may be due to the incorporation of GTP in the RGO suspension. Meanwhile, the MTT assay shows that the percent inhibition of cell proliferation of GTP-RGO-WR5 was lower than GTP-RGO-WR1 at a concentration of 6.25 µg/mL. This finding indicates that the incorporation of a higher amount of GTP resulted in a further decrease in toxicity of GTP-RGO samples. This result was further supported by the zero percent inhibition of cell proliferation by the GTP sample (at 6.25 µg/mL), which suggests the non-toxicological effect of GTP and its ability to reduce the toxicity effects of GTP-RGO samples.

Despite the promising results of GTP-RGO-WR1 and GTP-RGO-WR5 at low concentration (6.25 µg/mL), the inhibition of cell proliferation (45-60%) of these GTP-RGO samples at higher concentrations (100 and 200 µg/mL) indicates slightly toxic effects. The toxicological effects of GTP-RGO samples at higher concentrations could be reduced by adding biocompatible materials including chitosan, polyethylene glycol (PEG) and polyethylenimine (PEI) to the RGO suspension[49, 50].

Fig. 10(a-e) shows the micrograph images of the untreated CCD-18Co cells and the cells 48 hours after treatment with GO, GTP-RGO-WR1, GTP-RGO-WR5 and GTP samples with a concentration of 6.25 µg/mL, respectively. From Fig. 10(a), the untreated cells from the control group show the normal features of a healthy CCD-18Co cells[51], whilst, the morphology of the CCD-18Co cells was distorted post treatment with GO as illustrated in Fig. 10(b). This reveals significant inhibition in cell proliferation after treatment with GO even at low concentration (6.25 µg/mL). As depicted in Fig. 10(c), the morphology of the cells was slightly distorted compared to the untreated cells. This indicates that the GTP-RGO-WR1 possesses slightly toxic effect towards CCD-18Co cells at low concentration. The cellular morphologies and populations of the cells treated with GTP-RGO-WR5 and GTP were almost similar to that of the control group as shown in Fig. 10(d) and Fig. 10(e), respectively. These observations indicate that the GTP-RGO-WR5 and GTP are non-toxic toward CCD-18Co cells at low concentration. The results from the cytotoxicity testing have shown that GTP possesses the ability to reduce the toxicological effect of GTP-RGO suspensions. Although the results from the cytotoxicity testing are promising, more intensive in vitro and in vivo studies are needed to fully understand the interactions between GTP-RGO and living cells in a biological system before any clinical applications can be realised.

4. Conclusions

The utilisation of GTP as a reducing agent has resulted in the successful reduction of GO and the preparation of a stable and well-dispersed GTP-RGO suspension in aqueous media. As a

safer and more environmental-friendly reducing agent, GTP has been demonstrated to possess comparable reduction efficiency relative to standard reducing agent, N_2H_4.It was found that the epoxide removal from GO was initiated by the ring opening of epoxy groups due to the transfer of hydrogen atom from EGCG in GTP. Our frequency calculations also suggest that the GO reduction using GTP was more favourable to occur and took place faster than the reduction using N_2H_4. The cell culture experiments have shown that the incorporation of GTP resulted in the decrease of the toxicological effects of the GTP-RGO samples.

The RGO prepared using GTP in this study shows low toxicity toward human cells and therefore can be considered to be an attractive material for biomedical applications.

Acknowledgments

This work was financially supported by the Universiti Sains Malaysia-Research University (USM-RU) grant (Grant number: 814143). Muhammad Faiq Abdullah also acknowledges the support by a Fellowship from Universiti Malaysia Perlis (UniMAP).

Supporting Information

Supporting information available for the reaction energy profiles for the GO reduction using (a) GTP and (b) N_2H_4 calculated at the functional theory level of B3LYP/3-21G (Fig. S1.) and calculated total energies (E_{total}), entropies (S), Gibbs free energies (G), enthalpies (H) and zero-point energies (ZPE) for species investigated in this study at the functional theory level of B3LYP/3-21G (Table S1.).

References

1. Lam, K.-T. and G. Liang, in H. Raza (Eds.), Electronic Structure of Bilayer Graphene Nanoribbon and Its Device Application: A Computational Study, Springer, 2012, 509-527.
2. Stine, R., S.P. Mulvaney, J.T. Robinson, C.R. Tamanaha, and P.E. Sheehan, Analytical Chemistry, 85 (2012) 509-521.
3. Grande, L., V.T. Chundi, D. Wei, C. Bower, P. Andrew, and T. Ryhänen, Particuology, 10 (2012) 1-8.
4. Shen, H., L. Zhang, M. Liu, and Z. Zhang, Theranostics, 2 (2012) 283-294.
5. Cai, W., Y. Zhu, X. Li, R.D. Piner, and R.S. Ruoff, Applied Physics Letters, 95 (2009)
6. Lee, C., X. Wei, J.W. Kysar, and J. Hone, Science, 321 (2008) 385-388.
7. Sanchez, V.C., A. Jachak, R.H. Hurt, and A.B. Kane, Chemical Research in Toxicology, 25 (2012) 15-34.
8. Novoselov, K.S., A.K. Geim, S.V. Morozov, D. Jiang, Y. Zhang, S.V. Dubonos, I.V. Grigorieva, and A.A. Firsov, Science, 306 (2004) 666-669.
9. Kim, K.S., Y. Zhao, H. Jang, S.Y. Lee, J.M. Kim, J.H. Ahn, P. Kim, J.Y. Choi, and B.H. Hong, Nature, 457 (2009) 706-710.
10. Singh, V., D. Joung, L. Zhai, S. Das, S.I. Khondaker, and S. Seal, Progress in Materials

Science, 56 (2011) 1178-1271.
11. Park, S. and R.S. Ruoff, Nature nanotechnology, 4 (2009) 217-224.
12. Pham, V.H., H.D. Pham, T.T. Dang, S.H. Hur, E.J. Kim, B.S. Kong, S. Kim, and J.S. Chung, Journal of Materials Chemistry, 22 (2012) 10530-10536.
13. Park, S., J. An, I. Jung, R.D. Piner, S.J. An, X. Li, A. Velamakanni, and R.S. Ruoff, Nano Letters, 9 (2009) 1593-1597.
14. Stankovich, S., D.A. Dikin, R.D. Piner, K.A. Kohlhaas, A. Kleinhammes, Y. Jia, Y. Wu, S.T. Nguyen, and R.S. Ruoff, Carbon, 45 (2007) 1558-1565.
15. Wang, G., J. Yang, J. Park, X. Gou, B. Wang, H. Liu, and J. Yao, Journal of Physical Chemistry C, 112 (2008) 8192-8195.
16. Si, Y. and E.T. Samulski, Nano Letters, 8 (2008) 1679-1682.
17. Powell, J.H. and P.M. Gannett, Journal of Environmental Pathology, Toxicology and Oncology, 21 (2002) 1-31.
18. Wang, Y., Z. Shi, and J. Yin, ACS applied materials & interfaces, 3 (2011) 1127-1133.
19. Cooper, R., D.J. Morré, and D.M. Morré, The Journal of Alternative and Complementary Medicine, 11 (2005) 521-528.
20. Matthews, C.M., Proceedings (Baylor University Medical Center), 23 (2010) 142-144.
21. Akhavan, O., M. Kalaee, Z.S. Alavi, S.M.A. Ghiasi, and A. Esfandiar, Carbon, 50 (2012) 3015-3025.
22. Moulton, M.C., L.K. Braydich-Stolle, M.N. Nadagouda, S. Kunzelman, S.M. Hussain, and R.S. Varma, Nanoscale, 2 (2010) 763-770.
23. Nadagouda, M.N. and R.S. Varma, Green Chemistry, 10 (2008) 859-862.
24. Nune, S.K., N. Chanda, R. Shukla, K. Katti, R.R. Kulkarni, S. Thilakavathy, S. Mekapothula, R. Kannan, and K.V. Katti, Journal of Materials Chemistry, 19 (2009) 2912-2920.
25. Chen, Y., Y.D. Lee, H. Vedala, B.L. Allen, and A. Star, ACS Nano, 4 (2010) 6854-6862.
26. Wojtoniszak, M., X. Chen, R.J. Kalenczuk, A. Wajda, J. Łapczuk, M. Kurzewski, M. Drozdzik, P.K. Chu, and E. Borowiak-Palen, Colloids and Surfaces B: Biointerfaces, 89 (2012) 79-85.
27. Frisch, M.J., G.W. Trucks, H.B. Schlegel, G.E. Scuseria, M.A. Robb, J.R. Cheeseman, G. Scalmani, V. Barone, B. Mennucci, G.A. Petersson, H. Nakatsuji, M. Caricato, X. Li, H.P. Hratchian, A.F. Izmaylov, J. Bloino, G. Zheng, J.L. Sonnenberg, M. Hada, M. Ehara, K. Toyota, R. Fukuda, J. Hasegawa, M. Ishida, T. Nakajima, Y. Honda, O. Kitao, H. Nakai, T. Vreven, J. Montgomery, J. A., J.E. Peralta, F. Ogliaro, M. Bearpark, J.J. Heyd, E. Brothers, K.N. Kudin, V.N. Staroverov, R. Kobayashi, J. Normand, K. Raghavachari, A. Rendell, J.C. Burant, S.S. Iyengar, J. Tomasi, M. Cossi, N. Rega, J.M. Millam, M. Klene, J.E. Knox, J.B. Cross, V. Bakken, C. Adamo, J. Jaramillo, R. Gomperts, R.E. Stratmann, O. Yazyev, A.J. Austin, R. Cammi, C. Pomelli, J.W. Ochterski, R.L. Martin, K. Morokuma, V.G. Zakrzewski, G.A. Voth, P. Salvador, J.J. Dannenberg, S. Dapprich, A.D. Daniels, Ö. Farkas, J.B. Foresman, J.V. Ortiz, J. Cioslowski, and D.J. Fox, *Gaussian 09*. 2009, Gaussian, Inc.: Wallingford CT.
28. Kim, M.C., G.S. Hwang, and R.S. Ruoff, Journal of Chemical Physics, 131 (2009)
29. Li, J.L., K.N. Kudin, M.J. McAllister, R.K. Prud'homme, I.A. Aksay, and R. Car, Physical Review Letters, 96 (2006)
30. Gholami, F., S.H.S. Zein, L.-C. Gerhardt, K.L. Low, S.H. Tan, D.S. McPhail, L.M. Grover, and A.R. Boccaccini, Ceramics International, 39 (2013) 4975-4983.

31. Wang, K., J. Ruan, H. Song, J. Zhang, Y. Wo, S. Guo, and D. Cui, Nanoscale Research Letters, 6 (2011) 1-8.
32. Bourlinos, A.B., D. Gournis, D. Petridis, T. Szabó, A. Szeri, and I. Dékány, Langmuir, 19 (2003) 6050-6055.
33. Stankovich, S., R.D. Piner, X. Chen, N. Wu, S.T. Nguyen, and R.S. Ruoff, Journal of Materials Chemistry, 16 (2006) 155-158.
34. Liao, R., Z. Tang, Y. Lei, and B. Guo, Journal of Physical Chemistry C, 115 (2011) 20740-20746.
35. Zhao, Y., L. Chen, G. Yakubov, T. Aminiafshar, L. Han, and G. Lian, The Journal of Physical Chemistry B, 116 (2012) 13010-13016.
36. Yi, M., Z. Shen, X. Zhang, and S. Ma, Journal of Physics D: Applied Physics, 46 (2013) 025301.
37. Li, C., X. Wang, Y. Liu, W. Wang, J. Wynn, and J. Gao, Journal of Nanoparticle Research, 14 (2012)
38. Choi, W., I. Lahiri, R. Seelaboyina, and Y.S. Kang, Critical Reviews in Solid State and Materials Sciences, 35 (2010) 52-71.
39. Jeong, H.K., Y.P. Lee, M.H. Jin, E.S. Kim, J.J. Bae, and Y.H. Lee, Chemical Physics Letters, 470 (2009) 255-258.
40. Young, R.J. and I.A. Kinloch, in P. O'Brien (Eds.), Graphene and graphene-based nanocomposites, Vol. 1, Royal Society of Chemistry, 2013, 145-179.
41. Fernández-Merino, M.J., L. Guardia, J.I. Paredes, S. Villar-Rodil, P. Solís-Fernández, A. Martínez-Alonso, and J.M.D. Tascón, Journal of Physical Chemistry C, 114 (2010) 6426-6432.
42. Li, D., M.B. Müller, S. Gilje, R.B. Kaner, and G.G. Wallace, Nature Nanotechnology, 3 (2008) 101-105.
43. Konkena, B. and S. Vasudevan, Journal of Physical Chemistry Letters, 3 (2012) 867-872.
44. Luo, J., L.J. Cote, V.C. Tung, A.T.L. Tan, P.E. Goins, J. Wu, and J. Huang, Journal of the American Chemical Society, 132 (2010) 17667-17669.
45. Everett, D.H., in (Eds.), Basic Principles of Colloid Science, Royal Society of Chemistry, London, 1988, 243.
46. Lei, Y., Z. Tang, R. Liao, and B. Guo, Green Chemistry, 13 (2011) 1655-1658.
47. Keszei, E., in (Eds.), Chemical Thermodynamics: An Introduction, Springer, 2012, 354.
48. Gao, X., J. Jang, and S. Nagase, Journal of Physical Chemistry C, 114 (2010) 832-842.
49. Feng, L., S. Zhang, and Z. Liu, Nanoscale, 3 (2011) 1252-1257.
50. Yang, X., Y. Tu, L. Li, S. Shang, and X.M. Tao, ACS Applied Materials and Interfaces, 2 (2010) 1707-1713.
51. Kim, E.C., Y. Zhu, V. Andersen, D. Sciaky, H.J. Cao, H. Meekins, T.J. Smith, and P. Lance, American Journal of Physiology - Cell Physiology, 275 (1998) C988-C994.

Fig. 1. Schematic illustration of the structures of the reactants; (a) GO with epoxy group, (b) EGCG and the predicted products; (c) GTP-RGO-WR1, (d) galloyl-derived orthoquinone, (e) water that involved in the GO reduction process.

Fig. 2. (a) Digital images of GO (left) and GTP-RGO-WR1 (right). (b) UV-Vis absorption spectra of GO, and GTP-RGO-WR1 as a function of reaction time.

Fig. 3. FTIR spectra of GO and GTP-RGO-WR1.

Fig. 4. TGA curves of GO and GTP-RGO-WR1.

Fig. 5. UV-Vis absorption spectra of GTP-RGO-WR1 and N_2H_4-RGO-WR1.

Fig. 6. C1s XPS spectra of GO, GTP-RGO-WR1 and N_2H_4-RGO-WR1.

Fig. 7. The atomic structures for stationary points involved in the GO reduction using GTP.

Fig. 8. The atomic structures for stationary points involved in the GO reduction using N_2H_4.

Fig. 9. Effect of different concentrations of GO, GTP-RGO-WR1, GTP-RGO-WR5 and GTP samples on the metabolic activity of CCD-18Co cells line as measured using MTT assay. The data were presented as means ± standard deviation with probability value, $p < 0.05$ (each sample was examined in triplicate ($n = 3$)).

Fig. 10. Micrograph images of CCD-18Co cells line after 48 hours treatment with the samples; (a) control cells, (b) GO, (c) GTP-RGO-WR1, (d) GTP-RGO-WR5 and (e) GTP. The arrows show the location of the distorted cells line.

Table 1. Zeta potential and electrophoretic mobility values of GO, GTP-RGO-WR1 and N_2H_4-RGO-WR1. All samples were measured at pH=7.

Table 2. The enthalpy change, ΔH (kcal/mol), entropy change, ΔS (kcal/mol·K) and Gibbs free energy change, ΔG (kcal/mol) for stationary points involved in the GO reduction using GTP and N_2H_4 at 90°C. All of the thermodynamic quantities were calculated at the theory level of B3LYP/3-21G.

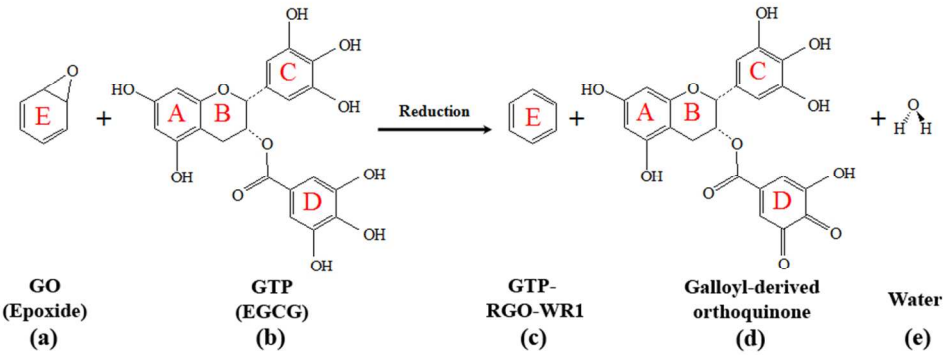

Fig. 1. Schematic illustration of the structures of the reactants; (a) GO with epoxy group, (b) EGCG and the predicted products; (c) GTP-RGO-WR1, (d) galloyl-derived orthoquinone, (e) water that involved in the GO reduction process.
346x127mm (72 x 72 DPI)

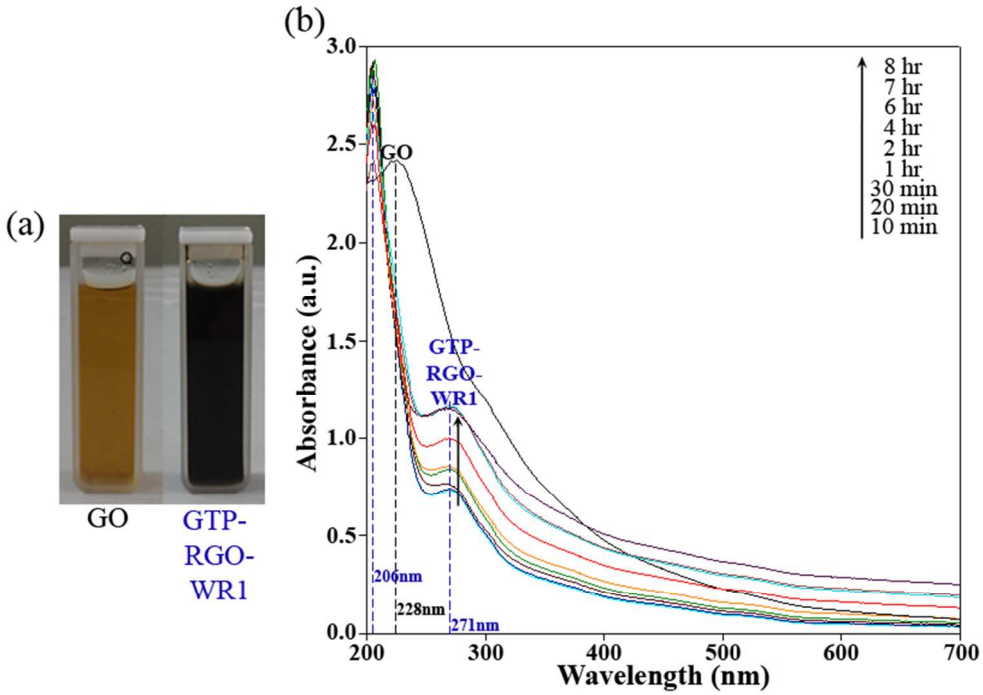

Fig. 2. (a) Digital images of GO (left) and GTP-RGO-WR1 (right). (b) UV-Vis absorption spectra of GO, and GTP-RGO-WR1 as a function of reaction time.
293x203mm (72 x 72 DPI)

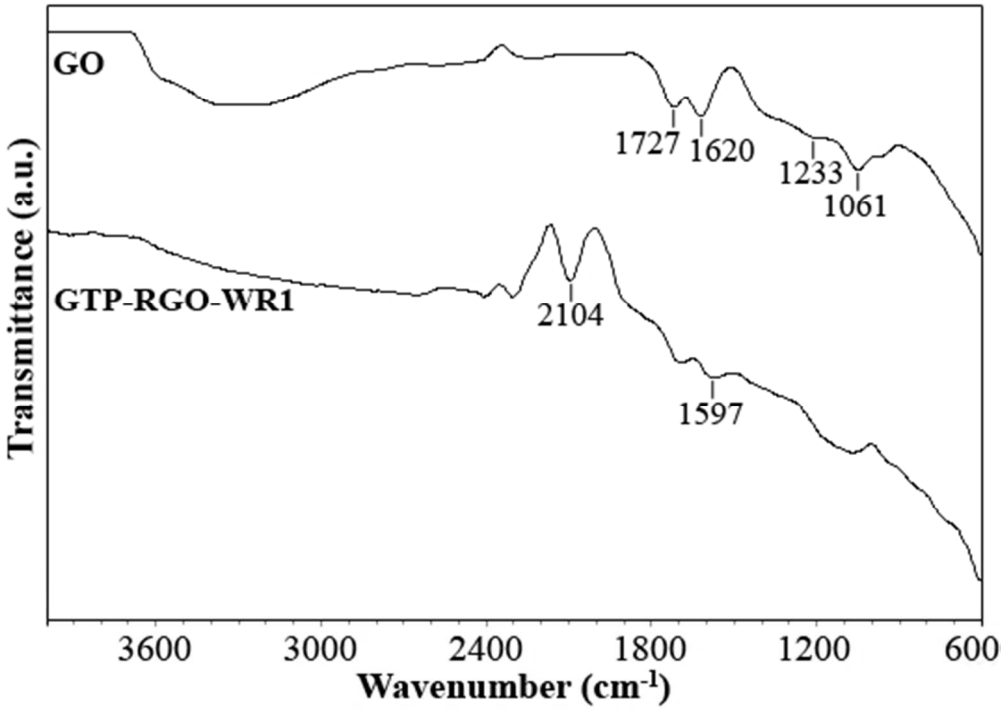

Fig. 3. FTIR spectra of GO and GTP-RGO-WR1.
189x136mm (72 x 72 DPI)

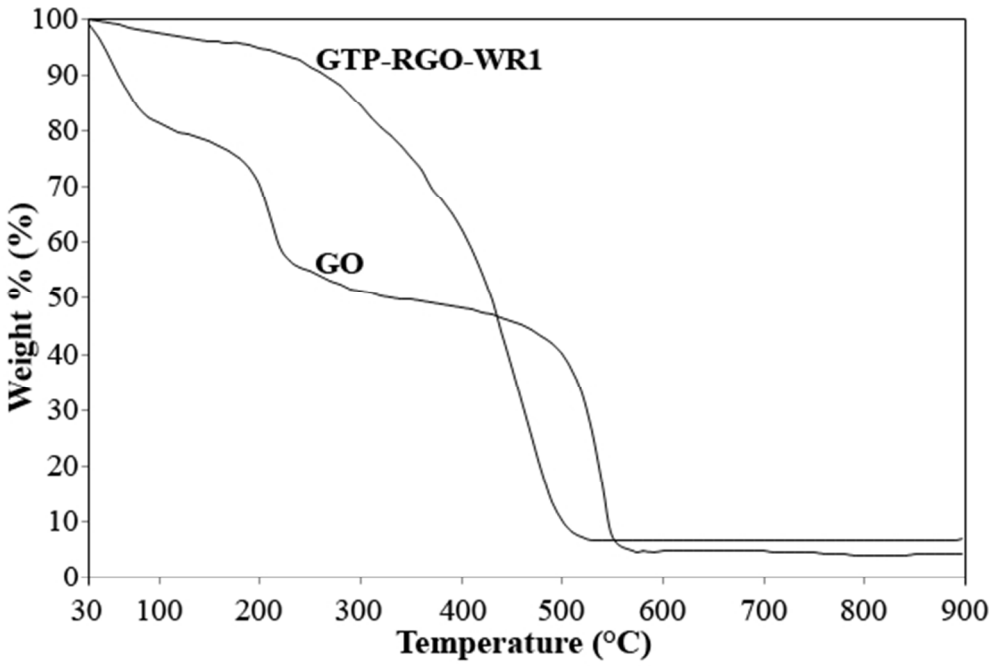

Fig. 4. TGA curves of GO and GTP-RGO-WR1.
156x104mm (96 x 96 DPI)

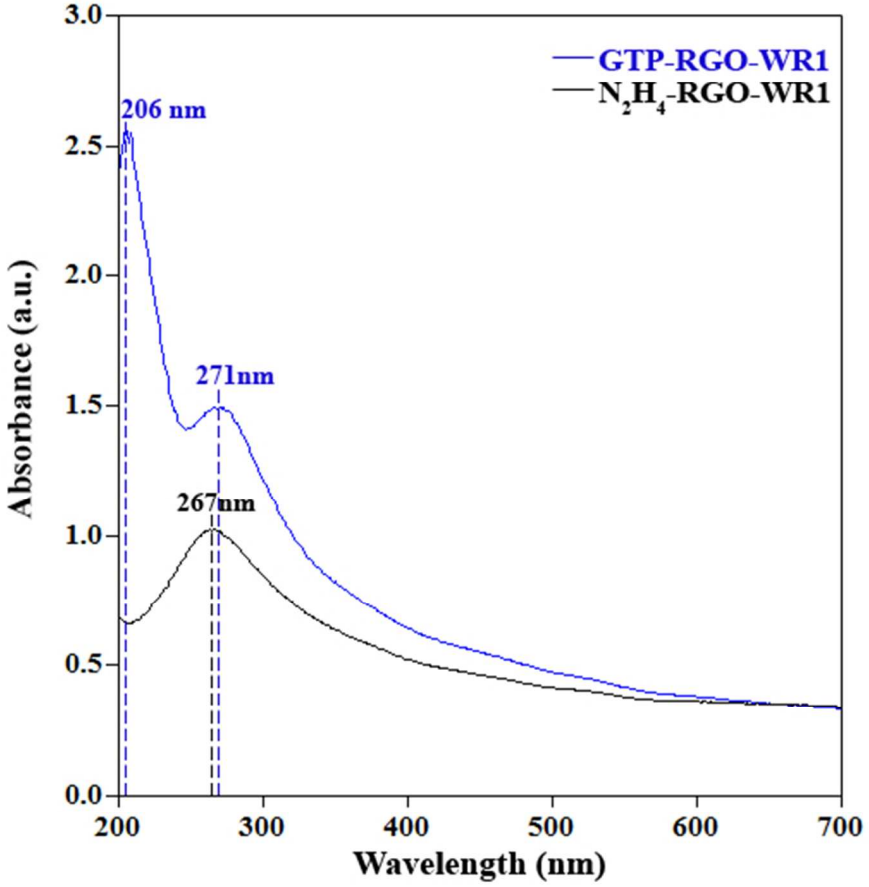

Fig. 5. UV-Vis absorption spectra of GTP-RGO-WR1 and N2H4-RGO-WR1.
153x144mm (96 x 96 DPI)

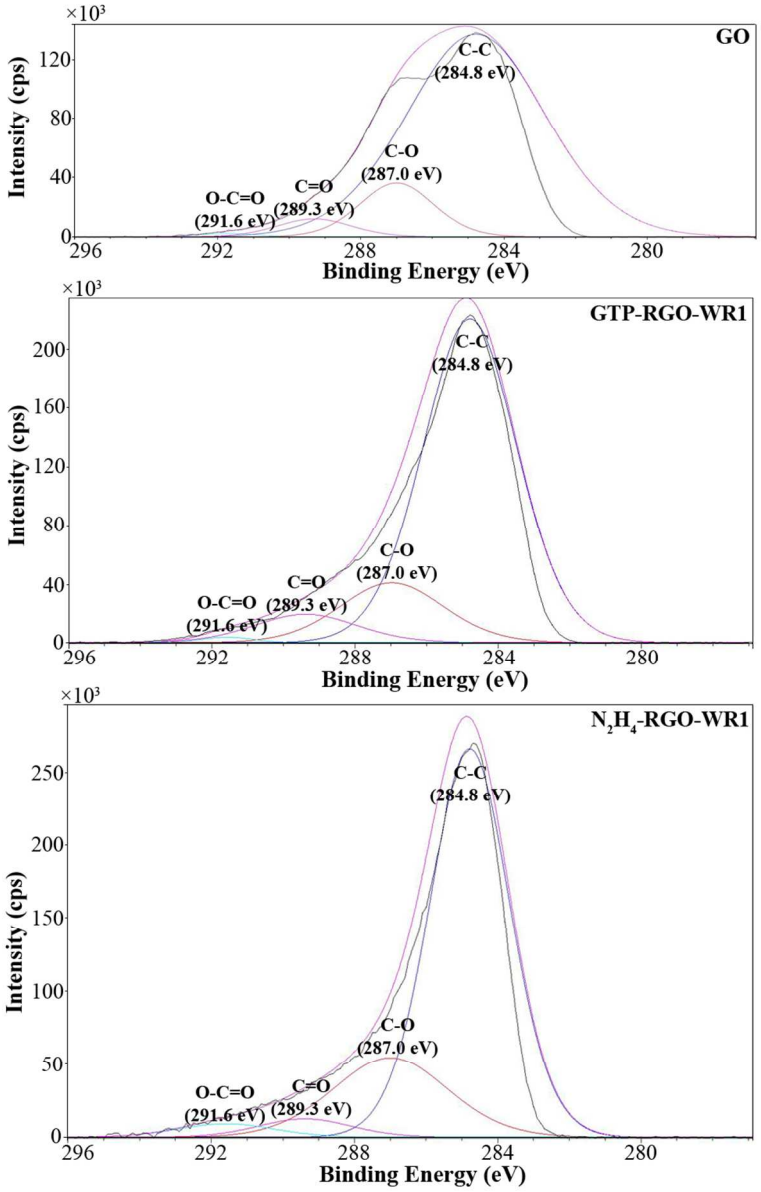

Fig. 6. C1s XPS spectra of GO, GTP-RGO-WR1 and N2H4-RGO-WR1.
348x541mm (72 x 72 DPI)

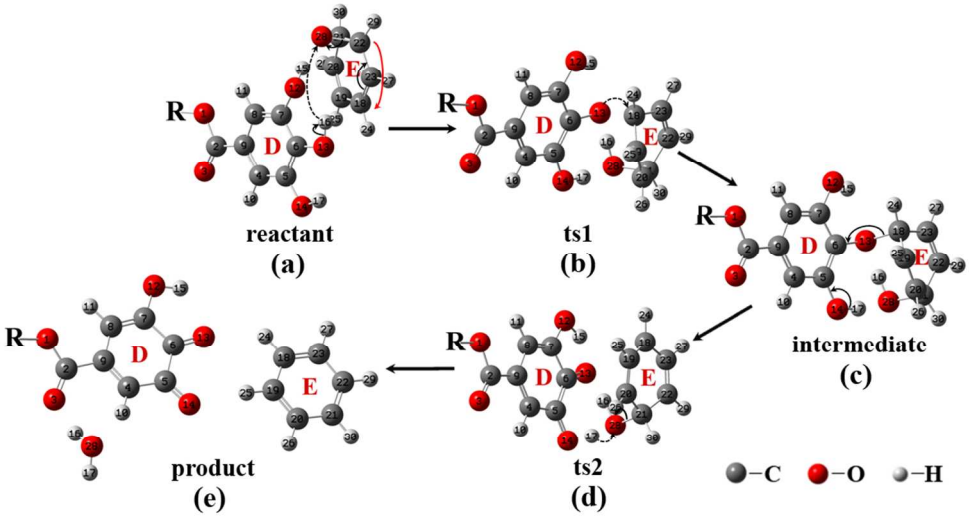

Fig. 7. The atomic structures for stationary points involved in the GO reduction using GTP.
428x236mm (72 x 72 DPI)

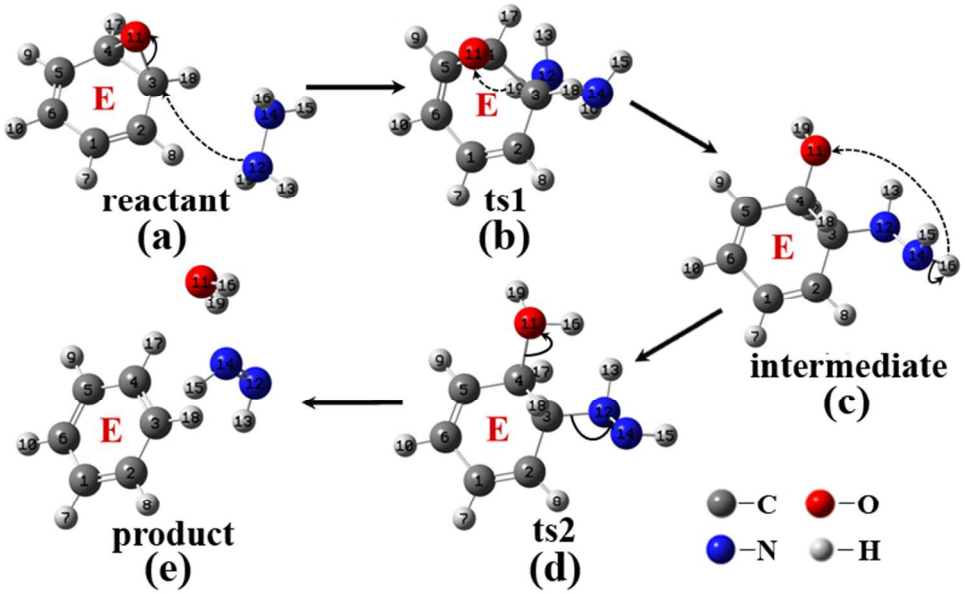

Fig. 8. The atomic structures for stationary points involved in the GO reduction using N2H4.
292x177mm (72 x 72 DPI)

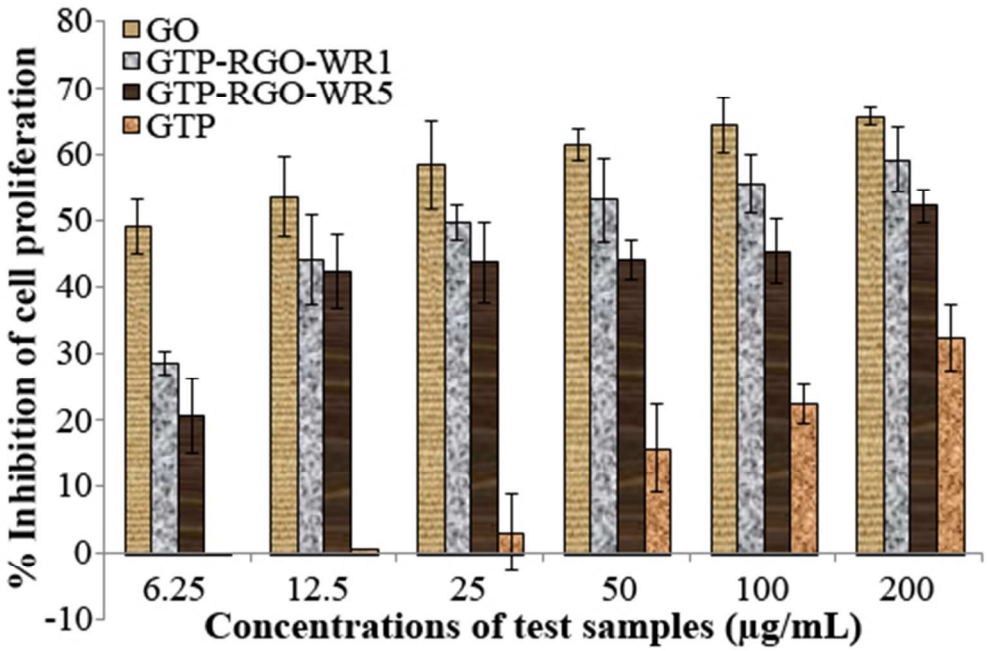

Fig. 9. Effect of different concentrations of GO, GTP-RGO-WR1, GTP-RGO-WR5 and GTP samples on the metabolic activity of CCD-18Co cells line as measured using MTT assay. The data were presented as means ± standard deviation with probability value, $p < 0.05$ (each sample was examined in triplicate (n = 3)).
135x88mm (96 x 96 DPI)

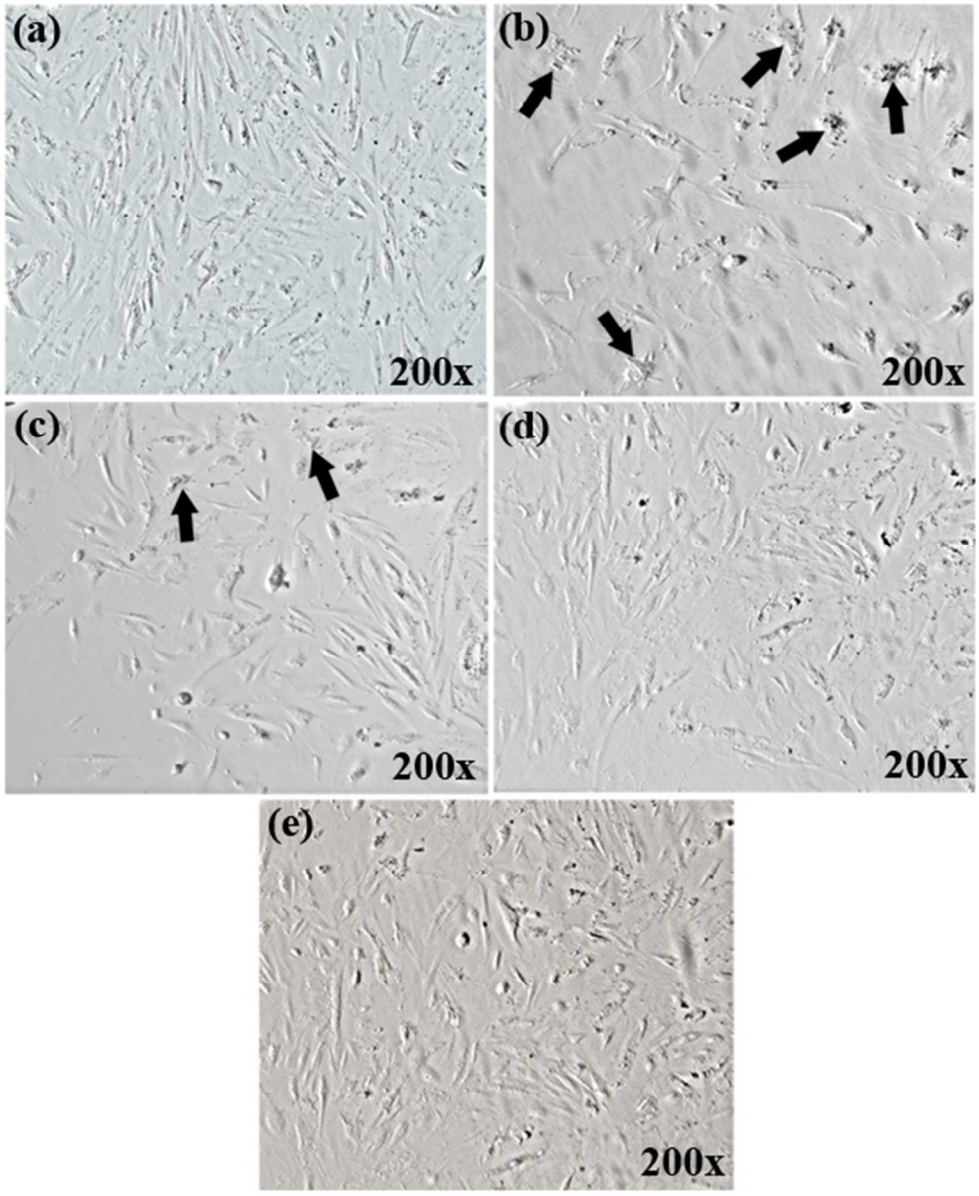

Fig. 10. Micrograph images of CCD-18Co cells line after 48 hours treatment with the samples; (a) control cells, (b) GO, (c) GTP-RGO-WR1, (d) GTP-RGO-WR5 and (e) GTP. The arrows show the location of the distorted cells line.
211x258mm (72 x 72 DPI)

Table 1. Zeta potential and electrophoretic mobility values of GO, GTP-RGO-WR1 and N_2H_4-RGO-WR1. All samples were measured at pH=7.

Sample	Zeta potential (mV)	Electrophoretic mobility (μmcm/Vs)
GO	-57.43 ± 0.72	-4.50 ± 0.06
GTP-RGO-WR1	-39.43 ± 2.16	-3.09 ± 0.17
N_2H_4-RGO-WR1	-15.50 ± 0.30	-1.21 ± 0.02

Table 2. The enthalpy change, ΔH (kcal/mol), entropy change, ΔS (kcal/mol·K) and Gibbs free energy change, ΔG (kcal/mol) for stationary points involved in the GO reduction using GTP and N_2H_4 at 90°C. All of the thermodynamic quantities were calculated at the theory level of B3LYP/3-21G.

	GO + GTP			GO + N_2H_4		
	ΔH	ΔS	ΔG	ΔH	ΔS	ΔG
reactant	0.000	0.000	0.000	0.000	0.000	0.000
ts1	9.204	-0.074	36.096	26.174	-0.042	41.354
intermediate	-35.020	-0.050	-16.773	-30.916	-0.041	-16.193
ts2	9.228	-0.074	36.107	68.122	-0.042	83.499
product	-14.053	0.039	-28.132	-16.021	0.035	-28.860

Supporting Information

Green tea polyphenol-reduced graphene oxide: Derivatisation, reduction efficiency, reduction mechanism and cytotoxicity

M. F. Abdullah[a, b], R. Zakaria[a],S. H. S. Zein[a, c,*]

[a]*School of Chemical Engineering, Engineering Campus, Universiti Sains Malaysia, 14300, Seri Ampangan, Nibong Tebal, Seberang Perai Selatan, Pulau Pinang, Malaysia*

[b]*School of Bioprocess Engineering, Universiti Malaysia Perlis, Kompleks Pusat Pengajian Jejawi 3, 02600, Arau, Perlis, Malaysia*

[c]*Department of Engineering, University of Hull, HU6 7RX, Hull, United Kingdom*

* Corresponding author. Tel.: +44 (0) 1482 466753.
E-mail address: S.H.Zein@hull.ac.uk (S.H.S Zein).

Contents

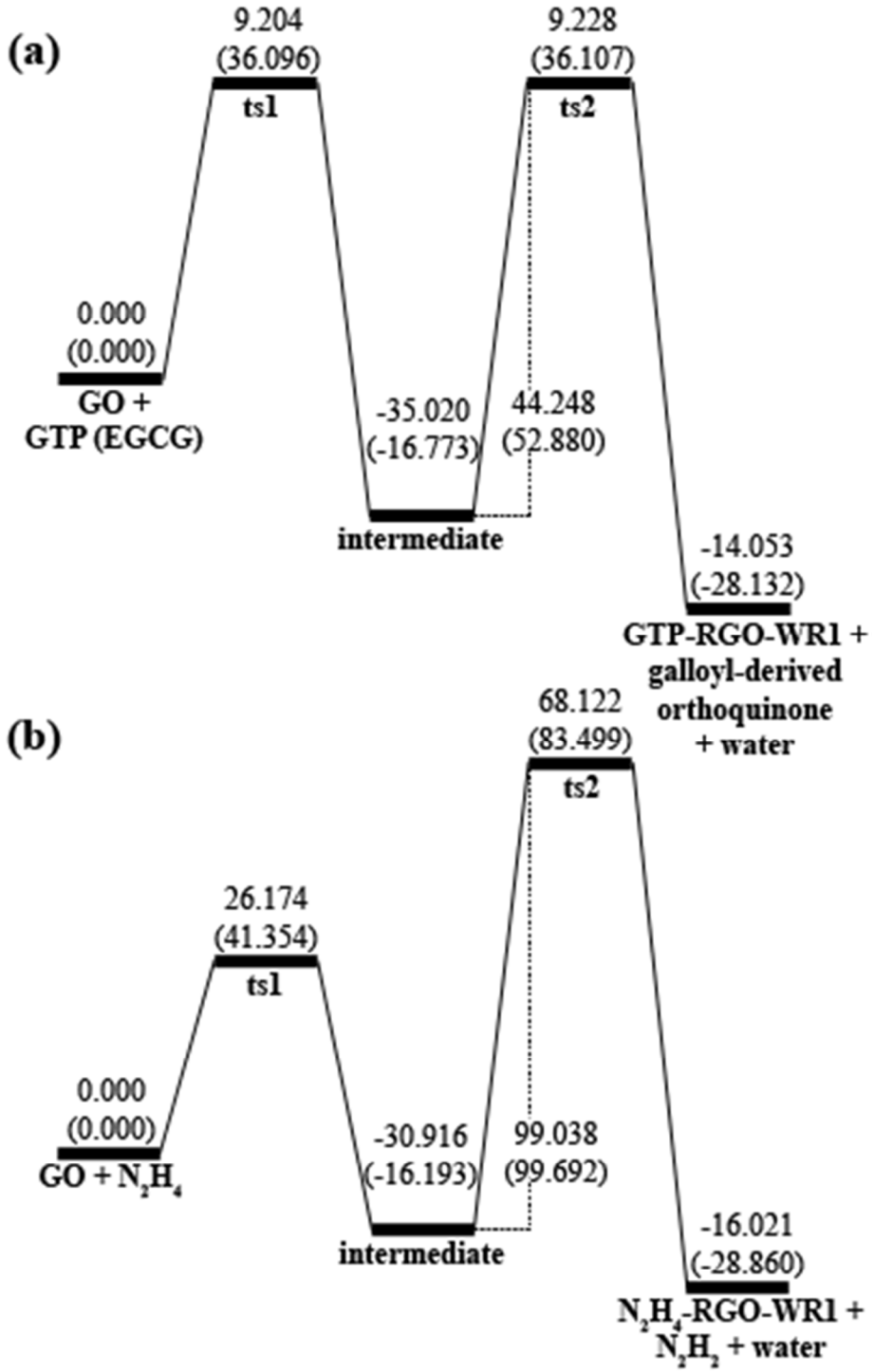

Fig. S1. Reaction energy profiles for the GO reduction using (a) GTP and (b) N_2H_4 calculated at the functional theory level of B3LYP/3-21G. The values of ΔH (kcal/mol) and ΔG (kcal/mol) at 90ºC were shown in normal typefaces without and with parentheses, respectively.

Table S1. Calculated total energies (E_{total}), entropies (S), Gibbs free energies (G), enthalpies (H) and zero-point energies (ZPE) for species investigated in this study at the functional theory level of B3LYP/3-21G.

	Species		E_{total} (a.u.)	S (cal.mol^{-1}K^{-1})	G (a.u.)	H (a.u.)	ZPE (a.u.)
GO + GTP (EGCG)	reactant	GO + epoxide	-305.5824	78.4650	-305.6267	-305.5813	0.1041
		EGCG	-1666.9518	215.0720	-1667.0751	-1666.9506	0.3773
	ts1		-1972.5184	219.4850	-1972.6443	-1972.5172	0.4703
	intermediate		-1972.5889	243.2910	-1972.7285	-1972.5877	0.4869
	ts2		-1972.5183	219.5220	-1972.6442	-1972.5172	0.4704
	product	GTP-RGO-WR1	-230.8678	72.8740	-230.9088	-230.8667	0.1017
		galloyl-derived orthoquinone	-1665.7392	212.5490	-1665.8610	-1665.7380	0.3547
		water	-75.9507	46.8830	-75.9767	-75.9496	0.0198
GO + N_2H_4	reactant	GO + epoxide	-305.5824	78.4650	-305.6267	-305.5813	0.1041
		N_2H_4	-111.1723	59.9340	-111.2058	-111.1711	0.0517
	ts1		-416.7119	96.5980	-416.7666	-416.7107	0.1574
	intermediate		-416.8029	97.8570	-416.8583	-416.8017	0.1596
	ts2		-416.6450	96.0560	-416.6995	-416.6439	0.1477
	product	N_2H_4-RGO-WR1	-230.8678	72.8740	-230.9088	-230.8667	0.1017
		N_2H_2	-109.9629	53.9950	-109.9930	-109.9617	0.0258
		water	-75.9507	46.8830	-75.9767	-75.9496	0.0198

*1 a.u. = 627.5 kcal/mol